Materials and Structures (2016) 49:4029–4048
DOI 10.1617/s11527-015-0771-7

ORIGINAL ARTICLE

Experimental and numerical study of size effect on long-term drying behavior of concrete: influence of drying depth

H. Samouh · A. Soive · E. Rozière · A. Loukili

Received: 15 October 2014 / Accepted: 21 December 2015 / Published online: 4 January 2016

Abstract This study aims at rationalizing the analysis of drying shrinkage tests and taking better advantage of the measurements, by studying the influence of the specimen size. Three self-consolidating concrete and one vibrated concrete mixes were studied during 3 years. Drying started 24 h after casting. The tests were carried on three sizes of cylinders: Φ78, Φ113 and Φ163 mm, under the same experimental conditions (20 ± 1 °C, 50 ± 5 % relative humidity), according to RILEM recommendations. The results show that the classification of concrete depends not only on the experimental conditions, but also on the duration of the shrinkage measurement. A scientific approach based on a simple mathematical model was proposed to analyze shrinkage data. The ultimate drying shrinkage did not depend on specimen size. The existing empirical models of shrinkage and drying used in construction codes take into account the size effect only through a geometrical parameter called notional size of cross-section, assuming that concrete is an homogeneous and non-aging material. With the time variable change by the ratio of the square root of the time and the notional size of cross-section, a master curve can be found for the theoretical curves of different sizes. However, experimentally, upshifts were observed between the drying shrinkage curves for different specimens sizes, thus phenomena that occur at early age are not taken into account by current models. The drying depth notion was introduced to explain the part of drying behavior responsible for the observed difference between drying curves. The influence of this concrete layer on the long-term behavior was confirmed by a two-step modeling of the mass-loss evolution. The first one included coupled drying-hydration model. The same classification was observed numerically and experimentally, with higher drying kinetics corresponding to smaller specimens, but the experimental shift could not be reproduced. The drying depth notion was incorporated in the second model; an increase in permeability was introduced in the outer layer of the concrete specimens. The size effect on the long-term mass-loss was reproduced numerically.

Keywords Self consolidating concrete · Drying · Shrinkage · Size effect · Drying depth

H. Samouh · A. Soive · E. Rozière · A. Loukili (✉)
Institut de Recherche en Génie Civil et Mécanique (GeM), Ecole Centrale de Nantes, UMR-CNRS 6183, Nantes, France
e-mail: ahmed.loukili@ec-nantes.fr

H. Samouh
Quille construction, Nantes, France

A. Soive
Centre d'Etudes et d'Expertises sur les Risques, l'Environnement, la Mobilité et l'Aménagement (Cerema), Nantes, France

1 Introduction

Drying and drying shrinkage are at stake in several degradation mechanisms of concrete and concrete structures. If restrained, drying shrinkage is likely to cause cracking. Thin walls and slabs of buildings are often reported to crack after a few months. The mitigation of drying shrinkage cracking requires a good understanding of the influence of mixture proportioning on the restrained cracking tendency of concrete in order to optimize the design of concrete mixtures [1, 2, 3]. Accurate prediction of time-dependent deformations, such as drying shrinkage and creep, is needed to assess the long-term deflection of big structures such as towers and bridges [4] and the losses in prestress. Durability is also influenced by drying and cracking [5]. The concrete cover protects steel reinforcement against the penetration of aggressive species from the environment to avoid corrosion. However in spite of a good curing the skin of concrete is generally exposed to drying before complete hydration, thus the porosity of concrete cover is higher than the porosity of internal concrete [6, 7], which leads to an increase in the permeability in the concrete cover. This effect can be increased by the wall effect due to formwork and compaction defects. Durability indicators are often assessed on undamaged specimens or cores, whereas cracks observed on structures can significantly alter the potential durability of structures [8, 9]. Thicker concrete covers are now prescribed to ensure durability in severe conditions, such as tidal zones in marine environments [10], but this is likely to increase cracks widths, thus permeability. Moreover the behavior of modern concrete mixtures, such as high strength concrete (HSC) or self-consolidating concrete (SCC) can significantly differ from the behavior of normal strength vibrated concrete (VC). As a consequence drying shrinkage limits are now included in performance-based specifications [11].

Since the beginning of the research about concrete drying shrinkage, two questions arose. The first one was the possibility to reproduce in the laboratory the drying conditions of the construction sites. Tests should be as representative as possible, to switch from the laboratory results to the structure scale. The second is how the tests can be accelerated and analyzed to deduce the long-term behavior of concrete. The size effect has been studied to answer these two questions. Since the 1960 s, several works have been published around this topic: Keeton studied the size effect on four specimen sizes during 1000 days [12]. Wallo & al. carried out experiments on three sizes over 100 days [13]. In order to study size effects, it is necessary to distinguish them from the effect of volume-to-surface (v/s) ratio. This analysis is generally done on shrinkage data, to deduce drying shrinkage of structural members from shrinkage curves of laboratory-size specimens. Torben proposed a hyperbolic equation to project shrinkage-time from test data [14]. Almudaiheem & al. gave equations to determine the fit parameters for the hyperbolical representation of shrinkage [15].They also gave a method to predict concrete drying shrinkage from short-time [16], and they studied the influence of major parameters on ultimate drying shrinkage [17]. The hyperbolic equation is still used in several models and standards, such as ACI 209 Code Model. Bazant & al. proposed a statistical extrapolation of shrinkage [18, 19]. The size effect analysis was not limited to vibrated concretes, but it also dealt with high strength concrete [20], with and without lightweight aggregates [21].

The influence of specimen size on drying shrinkage kinetics is generally taken into account through the notional size of cross-section concept, i.e. the volume-to-surface area ratio h_0.

$$h_0 = \frac{2v}{s} \tag{1}$$

where v is the volume and$s$ is the drying surface of the specimen. Most of models use this geometrical parameter to describe the influence of specimen size on the long-term behavior. For instance, the empirical modeling of the shrinkage with CEB [22], B3 [23], ACI [24], and Eurocode models derived from this ratio. They link it directly with the kinetics of shrinkage, by hyperbolical or exponential mathematical equations. However, the models do not agree on the relation between kinetics and notional size of cross-section. For instance, in Eurocode 2 part 1-1 for buildings, the time when shrinkage reaches half of ultimate drying shrinkage or "shrinkage halftime" is a linear function of $h_0^{2/3}$, whereas in Eurocode 2 part 2 for bridges and B4 model [25], it is a linear function of h_0^2. This linear function is valid only in 1D and if drying shrinkage is assumed be governed by a diffusion-equation, which can be discussed if cracking occurred. Moreover, mature concrete can be considered as homogenous material and described by simple

models based on notional size of cross-section, which is not the case when concrete is exposed to drying at short term, because of time and space evolution of concrete properties.

The general drying shrinkage equation given by several models, including code models implies that ultimate drying shrinkage also depends on specimen size (2).

$$\varepsilon_{ds} = \varepsilon_{ult.sh}(h_0, T, RH)\beta(h_0, t) \quad (2)$$

According to Torben, Hansen & Mattock [14] and Eurocode 2 part 1-1 [10], the ultimate shrinkage decreases with an increase in notional size of cross-section. However these models seem questionable [26]. The drying shrinkage increases very quickly at earlyage, thus relatively low measurement errors at early age are likely to cause significant variations of ultimate drying shrinkage [25]. The evolution of experimental devices facilitates testing and allows more frequent and more accurate measurements from early age and for longer periods. As a consequence the improvement of testing can provide some useful information on size effect. Moreover numerical tools now help understanding the long-term behavior of concrete and verifying assumptions on prevailing phenomena.

The issue addressed in this paper is the influence of the early-age drying and the coupling between hydration, damage, and drying on long-term drying and shrinkage of concrete. As the experimental study deals with relatively high water-to-cement (w/c) ratio concretes, the coupling between drying and autogenous shrinkage was not taken into account. When concrete is exposed to drying at early ages, i.e. after one or a few days, the hydration degree is relatively low, thus the permeability and kinetics of water loss are higher than mature concrete. Another consequence is that tensile strength is low, which favors micro-cracking, damage, and relaxation of tensile stress developing in the external layer of specimens [27], thus the long-term behavior, the kinetics, and the magnitude of shrinkage can be influenced by the phenomena occurring at early age.

The objective of this experimental and numerical study is to highlight and understand the size effect on long-term drying. It also provides experimental data on the influence of specimen size on kinetics and ultimate drying shrinkage. The proposed study dealt with SCC and VC.

The first part gives the concrete mixture proportions and the geometry of the specimens. Shrinkage and mass were measured from 24 h on three sizes of cylinders, Φ78, Φ113 and Φ163 mm, under the same experimental conditions (20 ± 1 °C, 50 ± 5 % RH) until the stabilization of values.

In the second part the experimental results are presented and discussed. First it is necessary to assess and eliminate the influence of notional size of cross-section to highlight the size effect. A hyperbolic equation is used to analyze the time evolutions and conclude on the effect of notional size of cross-section on ultimate value and kinetics of drying shrinkage. As the notional size of cross-section cannot fully explain the size effect, the drying depth concept is introduced. If drying was the only phenomenon involved in long-term behavior, a variable change could back the mass-loss and drying shrinkage curves into a master curve. Experimentally, this was not the case. Concrete is a complex material with aging properties due to drying and hydration evolution, in addition to micro cracks and skin effect. The combination of all these phenomena could explain the observed size effect. The shrinkage versus mass loss graphs helps to understand this behavior. The drying depth notion is introduced in this paper to facilitate its comprehension and to understand the size effect.

The third part of the paper deals with the numerical model used to understand the long-term drying of concrete. A tow-step modeling is performed. First the influence of the drying-hydration coupling is presented. Then the drying depth notion is integrated to the model to explain the size effect on drying.

2 Experimental program

2.1 Mixture proportions and mechanical properties

Four concrete mixtures were designed: three self-consolidating concrete (SCC), referred to as: SCC-N, SCC-R and SCC-G, and one normally-vibrated concrete (named VC). ACEM I 52.5 N Portland cement, limestone filler, and a polycarboxylate superplasticizer were used. The aggregates consisted of alluvial sand, amphibolite (SCC-G and VC) and limestone gravels (SCC-N and SCC-R). SCC-N and SCC-R were designed keeping the volume of paste and water

content constant but varying the limestone filler-to-cement ratio. SCC-R and SCC-G were designed keeping the proportions of paste content constant but varying the gravel type. VC and SCC-G mixtures were designed with the same gravel to observe the difference in long-term behavior between vibrated concrete and SCC, due to variations of the volume of paste and water-to-cement (W/C) ratio. The mix design proportions are given in Table 1.

The mechanical characteristics are assembled in Table 2. Young's modulus was determined by dynamic testing, using *Grindosonic* device and Spinner and Teft model [28]. This provides higher value than quasi static compressive testing (Neville, 2000).The Vibrated concrete had the highest Young's modulus, since it had the lowest paste volume [1]. SCC-N showed the lowest compressive strength due to the high limestone filler-to-cement ratio; it also showed the lowest autogeneous shrinkage after 5 months of measure owning to high W/C ratio. The substitution of the cement by limestone filler cannot results in lower chemical shrinkage from Portland cement hydration, the main cause of the auto-desiccation shrinkage. A small difference was observed between SCC-R and SCC-G, which can be explained by the effects of gravel nature, if amphibolite gravel is assumed to be stiffer than limestone gravel.

2.2 Specimens and testing procedure

SCC and VC were stable and showed no signs of segregation. In addition to compressive strength and Young's modulus measured on cylindrical specimens Ø113 mm, three cylindrical molds were used, to observe the size effect on long-term behavior. Cylinders dimensions and notional size of cross-section given by Eq. (1) [10] were respectively Ø78 mm ($h_0 = 39$ mm), Ø113 mm ($h_0 = 56.5$ mm), and Ø163 mm ($h_0 = 81.5$ mm) observing a proportionality factor 1.45.

In 1998, the RILEM Technical report [29] gathered some recommendations on the measurement of time-dependent strains of concrete. The experimental procedure was based on the advised procedure. The specimens were moved immediately after casting to an air-conditioned room, at 20 ± 1 °C and 50 ± 5 % RH, and demoulded 24 h later. The top and bottom surfaces were covered with an adhesive-backed aluminum foil, to achieve 2-dimension drying. The total drying shrinkage and mass-loss were measured on

Table 1 Mix design of SCC and VC

kg/m^3	SCC-N	SCC-R	SCC-G	VC
Limestone gravel 4/12 (G)	751	755	–	–
Amphibolite gravel 10/14 (G)	–	–	720	875
Amphibolite gravel 6/10 (G)	–	–	128	211
Sand 0/4 (S)	806	810	813	855
Cement (C)	258	320	320	303
Limestone filler (A)	292	230	230	–
Superplasticizer	3.8	3.8	3.6	–
Water (W)	190	190	190	182
V_G/V_S	0.9	0.9	0.9	1.1
W/C	0.74	0.59	0.59	0.60
W/P[a]	0.34	0.34	0.34	0.60
Volume of paste (l/m^3)	380	380	380	280

[a] Water-to-powder ratio, $P = C + A$

Table 2 Mechanical properties of SCC and VC

	SCC-N	SCC-R	SCC-G	VC
Compressive strength, 28 days (MPa)	32.6	49.6	48.0	49.1
Young's modulus, 28 days (GPa)	33.6	38.2	40.5	45.0
Autogenous shrinkage, 5 months (μm/m)	73	106	91	102

these specimens immediately (within 3 min) after removing the molds. LVDT sensors were used to measure the shrinkage strains. The specimens used to measure autogenous shrinkage were carefully protected against drying from the start of testing. Six months later, only an average of 0.03 % mass loss was observed on the sealed specimens. The use of a double layer of adhesive-backed aluminum foil is actually more effective than acrylic, latex, or epoxy protection [30]. The drying shrinkage was deduced as the difference between the measured total shrinkage and autogeneous shrinkage [31]. It is very important to respect this procedure for different specimens and concrete mixtures, because the internal humidity can change quickly at early age, and the concrete saturation affects the long-term behavior.

3 Experimental results and discussion

3.1 Analysis of drying shrinkage data

In many studies and specifications [11, 32] shrinkage magnitudes are used as criteria to classify concrete mixtures, although it is not an intrinsic parameter of the material. Figs. 1 and 2 show that the shrinkage magnitude does not only depend on the measurement duration, but also on the specimen size. The concrete classification changed with the specimen size. For example, the shrinkage of the VC was higher than the shrinkage of SCCs from the 1-month values on Ø78 mm specimens, whereas it was the lowest from the values on Ø163 mm specimens. Therefore a more reliable procedure is necessary to provide a concrete ranking independent from size effect and drying time.

According to most of shrinkage models, the evolution of shrinkage strain can be described by combining two functions: magnitude and kinetics. The kinetics decreases with notional size of cross-section. According to Eurocode 2 part 1-1 and Torben & al. [14], the ultimate shrinkage decreases with an increase in notional size of cross-section, but other models assume that the magnitude of shrinkage is not influenced by specimen size. In the study presented in this paper, the hyperbolic equation introduced by Torben & al. was used [14] (Eq. 3). The equation in the Code Model 2010 is similar, but uses the square root. In this case, the equation of the code model is more physical than the one proposed by Torben for mature concrete, as the shrinkage should be almost proportional to the square root of time at the beginning. The choice of Eq. 3 was based on a previous comparative study between different models, and a better fitting of experimental data was found with Torben's model [14].

$$\varepsilon_{dry} = \frac{t}{t + N_s}\varepsilon_{\infty} \tag{3}$$

The two parameters, ε_{∞} long-term drying shrinkage and N_s time to reach half of the long-term drying shrinkage, were determined from the experimental data so as to minimize the mean square error.

The shrinkage of the different concrete mixtures and specimens can be projected from the test data by assuming that the time evolution of drying shrinkage can be represented by Eq. (3). This equation form was

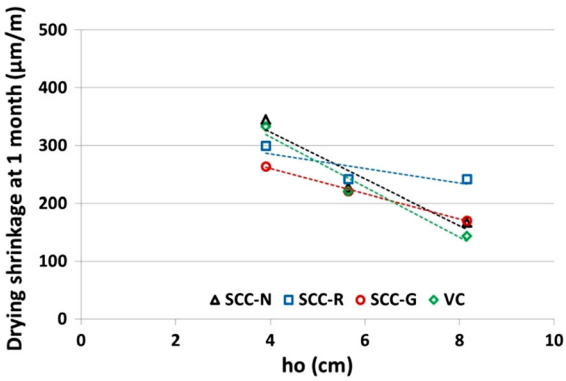

Fig. 1 Evolution of drying shrinkage at 1 month as function of notional size of cross-section

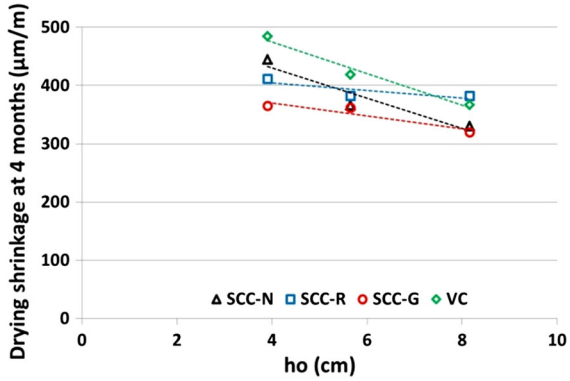

Fig. 2 Evolution of drying shrinkage at 4 months as function of notional size of cross-section

used in several international standards, such as American code model ACI 209R-92 [33] and European code model Eurocode 2 [10]. It has also been adapted for different concrete types like lightweight aggregate concrete [34] or SCC.

The drying shrinkage of the three SCC-G concrete specimens is plotted on the graph of Fig. 3. The measurements lasted between 120 and 800 days according to the specimen size. Figure 3 shows expected classification with a faster development of the drying shrinkage for the smaller specimen size. These results are in agreement with many works [12, 13, 14, 18, 19, 15, 35].

The couples (ε^{∞}, N_s) were determined for all mixtures and specimen sizes. Both parameters were plotted as a function of the square of the notional size of cross-section (see Figs. 4, 5). The smallest specimens are most sensitive to variations of external conditions, thus one repeatability test was performed on the VC mixture with two specimens (Φ78 mm). The results showed 1.2 days average deviation for Ns, and 25 µm/m average deviation for ultimate shrinkage. Error bars have been plotted in Figs. 4 and 5. The long-term drying shrinkage deduced from experimental data was not significantly influenced by specimen size. The difference between long-term shrinkage values of different specimen sizes varied between 15 and 49 µm/m for the four concrete mixtures (Fig. 5), which is consistent with the assumption made in models that the shrinkage magnitude does not depend on specimen size. However the kinetics of shrinkage clearly depends on the notional size of cross-section, since N_s increased with h_0, especially for the vibrated concrete. This means VC needed more time to reach the ultimate shrinkage than the SCC, thus the drying of paste was affected by the relatively high aggregate proportion of the VC mixture.

Several relations were proposed in the literature [16] to describe the influence of notional size of cross-section on N_s time. A classical approach is to consider that N_s depends linearly on the square of the notional size of cross-section, as proposed in ACI 209R-92 [33] (see Eq. (4)). This linearity allows a variable substitution, and a new formulation of drying shrinkage equation can be obtained, with a parameter independent from notional size of cross-section:

$$N_s = ah_0^2 \tag{4}$$

N_s was substituted to the equation:

$$\varepsilon_{dry} = \frac{t}{t + ah_0^2}\varepsilon_{\infty} \tag{5}$$

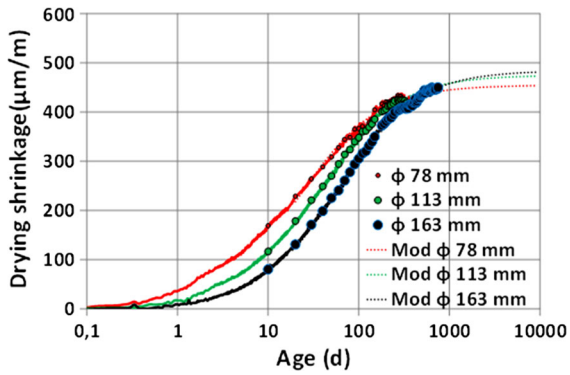

Fig. 3 Drying shrinkage versus log(t) forSCC-G

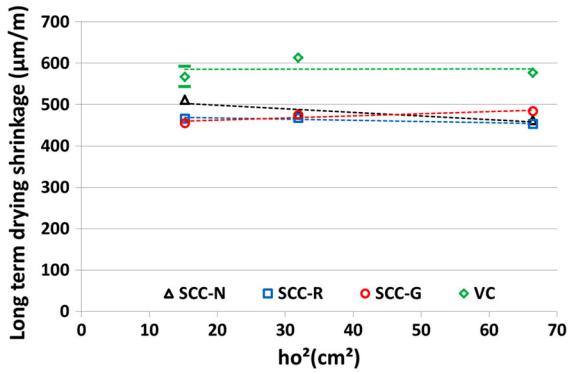

Fig. 4 Long-term drying shrinkage versus the square of the notional size of cross-section

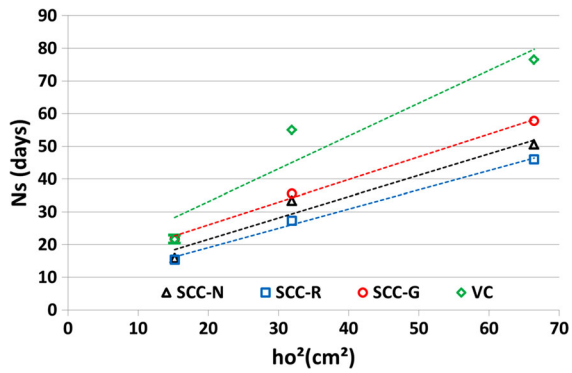

Fig. 5 Ns versus the square of the notional size of cross-section

With a variable change:

$$t^* = \frac{\sqrt{t}}{h_0} \quad (6)$$

Shrinkage can be rewritten as:

$$\varepsilon_{dry} = \frac{t^{*2}}{t^{*2} + a}\varepsilon_\infty \quad (7)$$

According to this last form of the drying shrinkage equation, the shrinkage versus t^* curves correspond to a unique master curve for the different sizes. Figure 6 shows the shrinkage as a function of t^*. A small shift between the different sizes was observed. The time t^* to reach ultimate drying shrinkage was higher for the thinnest specimens. These differences may mean the existence of other phenomena not taken into account by the linear variation of N_s as a function of h_0.

Assuming an affine function of $h_0^2(N_s + ah_0^2 + \beta, \beta \neq 0)$ rather than a linear function ($\beta = 0$, see Fig. 5) as proposed in Eq. (4) actually leads to a drying shrinkage that depends on sample size, even if notional size of cross-section has been taken into account (see Eq. (8)). In this case, the experimental results can be understood. Despite the variable change, the drying shrinkage still depends on h_0. The drying shrinkage time N_s thus obtained is actually higher, especially for low notional size of cross-section, which is in agreement with the experimental data (Fig. 6).

$$\varepsilon_{dry} = \frac{t^{*2}}{t^{*2} + a + \beta/h_0^2}\varepsilon_\infty \quad (8)$$

3.2 Mass-loss and drying shrinkage relation

The drying shrinkage is due to water loss, thus mass loss and drying shrinkage versus mass loss relations must be studied to understand drying and shrinkage. Mass loss also depends on initial and boundary conditions.

The mass-loss versus t^* curves were plotted to distinguish the effect of notional size of cross-section from the size effect. This corresponds to the variations observed on drying shrinkage versus t^* curves [36]. If drying was the only phenomenon, a superposition of the three curves would be observed. If the material is homogeneous, water loss can be modelled by drying equations (like the heat or diffusion equations), and the solution of this problem in 1-D for different sizes can be described by previous variable change to pass from one size to another. As shown in Figs. 7, 8, 9, 10 an upshift was observed for Ø78 mm specimens. The existence of phenomena parallel to drying was proved for the four mixtures tested here. These phenomena gave an additional kinetic for the smaller specimens, but keep the long-term mass-loss constant between all sizes. It is also interesting to note that the difference between the kinetics of the small and the medium

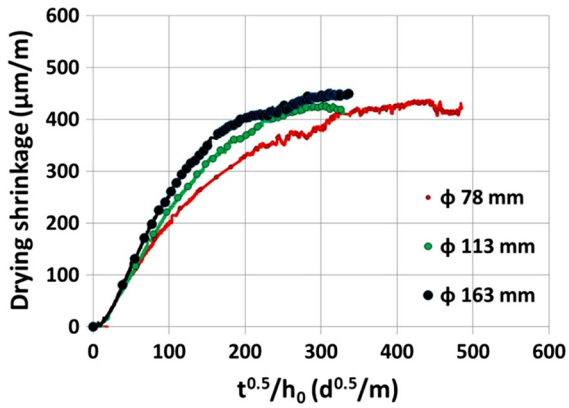

Fig. 6 Drying shrinkage versus t^* for SCC-G

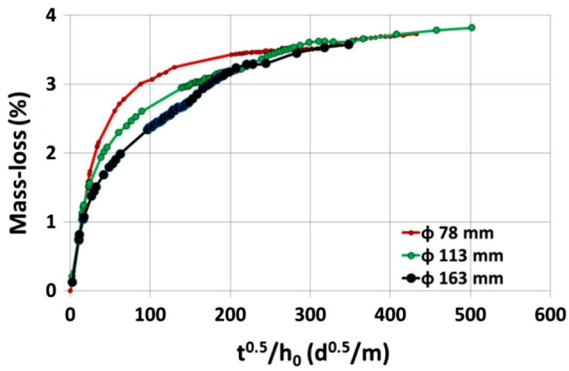

Fig. 7 Mass-loss versus t^* for SCC-N

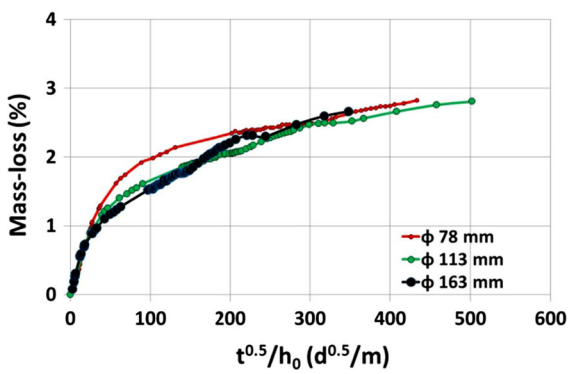

Fig. 8 Mass-loss versus t^* for SCC-R

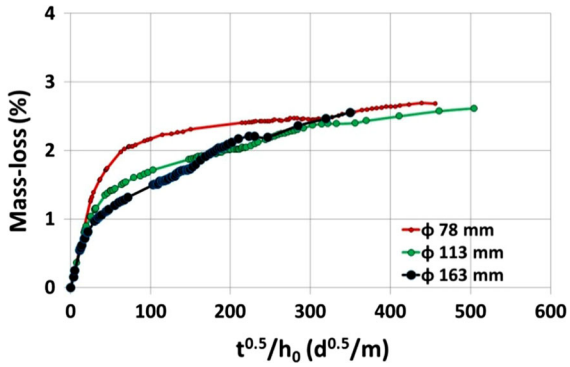

Fig. 9 Mass-loss versus t^* for SCC-G

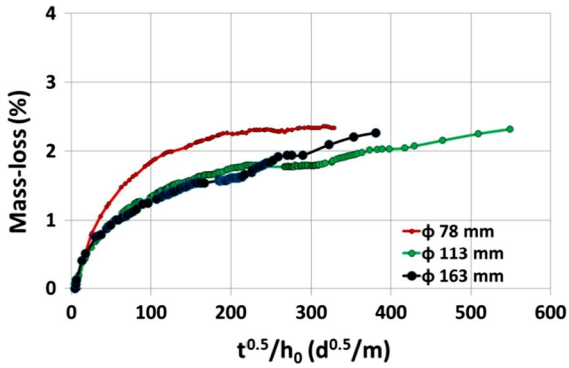

Fig. 10 Mass-loss versus t^* for VC

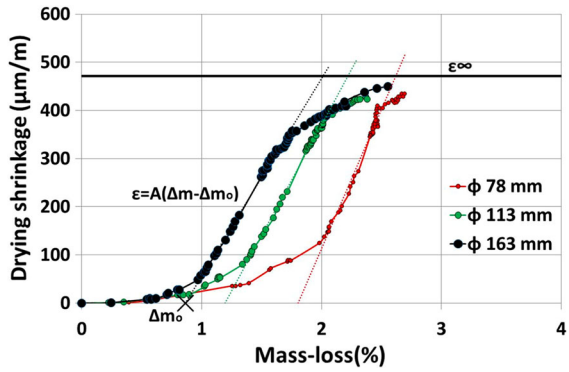

Fig. 11 Drying shrinkage versus mass-loss for SCC-G

samples was always greater than the difference between the kinetics of the medium and the big samples. The microstructure of concrete, at the level of capillary pores, can be expected to play a significant part in this size effect.

The curves given in Figs. 7, 8, 9, 10 also show the influence of the proportions of concrete mixtures. *SCC-N* was the concrete mixture with the highest limestone filler proportion; it lost the highest water amount, owing to the chemical nature of the addition, which leads to a higher proportion of free water ($w/c = 0.74$). *SCC-R* and *SCC-G* showed the same ultimate mass loss. Both concrete mixtures actually had the same water, cement, and filler contents. The gravel type did not significantly influence their drying behavior. *VC* showed the lowest ultimate mass loss, as the concrete mixture had the lowest water content.

In Fig. 11, drying shrinkage is plotted against weight loss for *SCC-G* mixture and all sizes. Several studies describe this curve as a linear relation [15, 37, 38]. In this study, a sigmoid function would be more appropriate to describe this relation. Three stages were observed. The first was a short stage with a mass loss up to 1 % without drying shrinkage. During this stage the measured total shrinkage and autogeneous shrinkage were equal; this phase depends clearly on the free water content of concrete mixture. The capillary stress due to this initial waterloss is not significantly higher than that created by hydration. This first stage corresponding to Δm_0 was longer for *SCC-N* than the other mixtures (Table 3) due to the high free water content. The second stage corresponds to a linear relation between shrinkage and mass-loss. The value of the slopes A generally increased when the sample size decreased (see Table 3). According to Kelvin-Laplace Eq. (9) the capillary stress decreases with the pore radius, therefore, shrinkage decreases also with the pore radius. *SCC-N* would have larger pores than the other concretes due to the significant departure of the free water Δm_0 and the relatively low value of the coefficients A. Whatever the concrete mixture, the biggest specimen showed more shrinkage for a given mass-loss. Finally, the third phase, which extends over a long period, represents an asymptote for the curves. Mass loss actually continued with a smaller shrinkage.

3.3 Size effect analysis

Because of the lack of experimental results, the influence of the early drying on the long-term behavior is rarely questioned. The experimental campaign performed during 3 years with reproducible results (faster mass loss kinetics for small specimens as shown in Figs. 7, 8, 9, 10) allows the verification and even validation of models present in the literature.

Table 3 The fit parameters of the linear trend curves

	Ø78 mm			Ø113 mm			Ø163 mm		
	A (μm/m)	Δm_0 (%)	t (Δm_0) (days)	A (μm/m)	Δm_0 (%)	t (Δm_0) (days)	A (μm/m)	Δm_0 (%)	t (Δm_0) (days)
SCC-N	381.6	2.34	3	278.5	1.83	4	256.2	1.34	4.4
SCC-R	381.6	1.37	2.6	372.1	0.99	3	362.6	0.83	4.4
SCC-G	578.8	1.80	3.8	459.8	1.19	3.8	410.7	0.86	5
VC	415.0	1.24	4.4	492.3	0.87	7	533.8	0.77	7

Classical models succeed in retrieving the classification of the kinetics according to notional size of cross-section, as well as long-term water loss. The remaining issue concerns the presence of other phenomena affecting the mass loss of the concrete, since the graphs show an offset in the experimental results when the abscissa axis is expressed in the square root of time to notional size of cross-section ratio t^* (Figs. 6, 7, 8, 9, 10). The classification is inversed as well, i.e. decreasing with the specimen size.

An assumption must be made about coupling physical and chemical phenomena, to explain the size effect observed on the mass-loss and shrinkage against t^* curves, which is not taken into account by classical models. This hypothesis consists in stating that two phenomena act in two opposite ways: hydration, which represents in this study a reduction of the porous volume (experimentally observed in [39]), and drying, considered as a water loss, which can cause the hydration reaction to stop at a certain level. These two phenomena compete, since the advance of one slows the other or even stops it. However, the two phenomena act in the same direction for drying shrinkage. According to the Kelvin-Laplace equation, they both cause higher capillary stresses, thus generating shrinkage, either by reducing internal relative humidity or reducing the pore radius. These combinations of both effects can be observed clearly on high-performance cementitious materials [31].

$$\sigma_{cap} = P_g - P_L = -\frac{RT\rho_e}{M}\ln(h) = \frac{2\sigma}{r}\cos(\alpha_m) \tag{9}$$

where σ_{cap}, Pg, P_L, R, T, M, ρ_e, h, σ, r and α_m: denote capillary stress, gas pressure, liquid pressure, universal ideal gas constant, temperature, molar mass of water, water density, humidity, surface tension of pore fluid, pore curvature and contact angle, respectively.

In order to understand the behavior of the samples as a function of size, the existence of a "drying depth" in concrete for which water loss is observed without generating shrinkage can be proposed, from the analysis of experimental results (Fig. 11). This "depth" is a concrete layer where the material dries quickly after demolding at 24 h, before it has reached high hydration degree. This zone is defined as the part of concrete which loses quickly the free water, corresponding to the first stage of the shrinkage versus mass loss graphs. This matches water loss in the specimens without measurable desiccation shrinkage, as shown in Fig. 11. This stage depends on concrete mixture. This representation can include several phenomena that can lead to the observed drying-shrinkage behavior, namely: coupling between hydration and drying [40], micro cracks [27, 41] and wall effect due to formwork [42, 43]. However, these phenomena cannot be easily distinguished.

A method is given to deduce this parameter directly from the shrinkage versus mass loss curves, by transforming the mass-loss to a distance. This operation can be made by a simple division of the mass-loss to drying surface ratio by the free water content of concrete, which depends on the concrete mixture. This ratio is noted here $d(10)$. The drying depth δ is defined as the intersection between the linear extrapolation of the second stage and the d-axis in the drying shrinkage versus d curve, as shown in Fig. 12.

$$d = \frac{m(t) - m(t_0)}{m_f * S_d} \tag{10}$$

$(m(t)-m(t_0))$: mass-loss (kg), S_d drying surface (m^2), m_f free water mass in 1 m^3 of concrete (kg/m^3).

The free water content is given by Eq. (11). W is the effective water content given in Table 1 (kg/m^3), α is the hydration degree at 24 h (when concrete is exposed to drying) determined by isothermal calorimetric

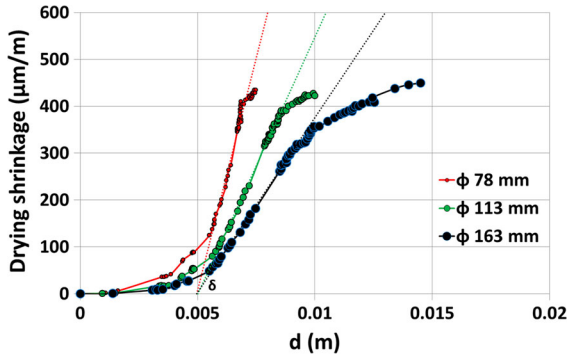

Fig. 12 Drying shrinkage versus d for SCC-G

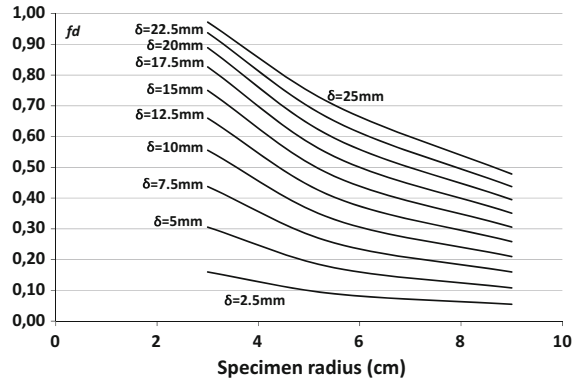

Fig. 13 Drying fraction evolution as function of the specimen radius and the drying depth

analysis, w_∞ is the ultimate value of the chemically bound water-to-cement content ratio (kg/kg), C is the cement content given in Table 1 (kg/m^3). α is assumed to be the same for the four concrete mixtures; the value is 0.4. The value of w_∞ equal to 0.25 was determined from the Bogue's composition of Portland cement.

$$m_f = W - \alpha W_\infty C \tag{11}$$

The results of this analysis for the three specimen sizes and the four mixtures are given in Table 4. The drying depth is weakly dependent on the specimen size, as shown by the standard deviation interval: from 0.0 to 0.6 mm for the four mixtures. The drying depth was higher for *SCC-N* than other concretes, and it can be explained by the high limestone filler proportion and low cement content of this mixture resulting in high free water in the concrete.

Assuming the drying depth is constant for a given concrete mixture, a simple calculation can be done to relate the "dry volume" (corresponding to the drying depth, not taking part in the stresses developed in the concrete) to the total volume of the specimen. This ratio, noted f_d, is defined by (see Eq. (12)):

$$f_d = \frac{v_{dry}}{v_{tot}} = 2\frac{\delta}{R} - \left(\frac{\delta}{R}\right)^2 \tag{12}$$

This ratio is plotted as a function of the specimen radius for different drying depths in Fig. 13. We note that for every value of δ, the difference between the ratios for radii 39 and 56.5 mm is always higher than the difference between the ratios for radii 56.5 and 81.5 mm, even though the radius difference increases. This is consistent with the size effect observed on shrinkage (Fig. 6) and drying (Figs. 7, 8, 9, 10), which was more pronounced between small and medium specimens than between medium and large specimens.

The reasoning proposed hereafter is meant to explain the influence of drying depth on drying shrinkage, by comparing two specimens of different sizes. For a given drying depth, the smallest specimen has a higher dry volume ratio as shown in Figs. 13 and 14. The drying depth has actually been defined as the concrete layer drying before causing significant drying shrinkage (Fig. 12), thus the mass lost without shrinkage, expressed in proportion of the specimen initial mass loss, increases as the specimen size decreases (Fig. 11).

Consequently, if hydration is assumed to be influenced by drying, a higher drying fraction of the small specimen leads to a coarser porosity. This allows the small specimen to dry quicker, thus explaining the

Table 4 Calculated drying depth for different concrete

δ (mm)	Ø78 mm	Ø113 mm	Ø163 mm	Average (mm)	Standard deviation (mm)
SCC-N	6.3	7.4	7.6	7.1	0.6
SCC-R	3.8	4.2	4.9	4.3	0.4
SCC-G	5.0	5.0	5.0	5.0	0.0
VC	3.4	4.0	4.9	4.1	0.5

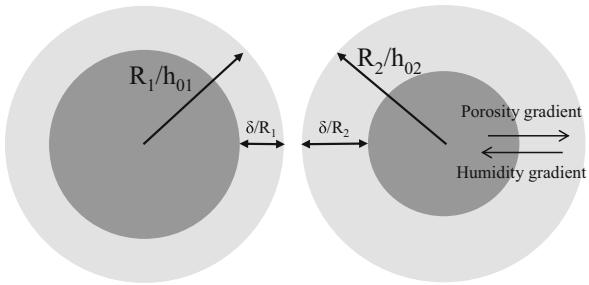

Fig. 14 The largest specimen in the left and the smallest specimen in the right ($R_2 < R_1$) reduced to a unit volume

positive offset of the mass loss graph, noted in Figs. 7, 8, 9, 10. The coarser the porous network, the faster the mass loss. For an equivalent water loss, the developed capillary stresses are actually lower, according to the Kelvin-Laplace Eq. (9). This interpretation is experimentally confirmed by the Fig. 6, showing an offset between the three curves, in opposite to the mass loss. The drying fraction could also explain the small difference observed in the transition part between the first phase and the second phase on drying shrinkage against mass-loss curves. The pore radius was actually larger for Φ78 mm, then for the same mass-loss, the shrinkage is lower (Fig. 11).

Analysis described in this paper provides a physical explanation to a size effect observed in experimental results of mass loss and shrinkage. This effect is generally neglected in mainstream model codes that deal with the drying of concrete. We can prove, by means of simple calculations that use the concept of drying depth that some additional phenomenon adds up to the effect of the water transport resulting in an increase of drying kinetics in smaller specimens. This variation can exceed 25 % between the smaller and the biggest specimen, concerning relative mass loss. The same phenomenon leads to lower shrinkage kinetics in smaller specimens. This concept can be very useful to describe the effect of the extreme conditions (high temperature or low relative humidity) when the size effect on shrinkage strain is likely to be more pronounced, as observed on experimental results [44].

4 Confirmation of the drying depth theory by hydration-drying model

Numerical models are generally used to determine relative humidity and saturation profiles in concrete. Then a linear relation between shrinkage and humidity variation or water loss is assumed at the micro-scale used to predict shrinkage of specimens or structures [38, 27, 45]. In this study drying shrinkage can be considered as input data to investigate the size effect on long-term drying. Shrinkage data were actually used first to eliminate the v/s effect, then to define the drying depth from shrinkage versus mass loss curves. Drying depth corresponds to the limit between the first and the second stage of drying, thus it integrates phenomena occurring at early age as well as long-term behavior. However the analysis of experimental data in part 3 cannot explain which phenomena caused the development of drying depth. The model described in this part was used to investigate two assumptions: the drying-hydration coupling at early-age, and the influence of porosity and permeability of external layer of concrete. These latter effects due to cracking of the external surface [17, 15] or a skin effect (less aggregate in the drying layer) were then taken into account by applying different transport properties between the drying depth and the center of the samples. Numerical results are given and compared with the experimental data.

The numerical model presented here has been developed based on previous works [46, 40, 47]. These studies underline the effect of the decrease of relative humidity due to drying or autogenous self-desiccation during or after concrete curing on hydration and moisture transport process. They propose mechanistic models (or at least mechanistic-type models) that take into account a full coupling between hydric phenomena and hydration, as well as changes of concrete properties caused by hydration process. It was preferred to phenomenological models in which no distinction is made between different phases of moisture [48]. It is actually difficult to take into account some changes of material properties, e.g. porosity, permeability, because they are lumped in

some model parameters. It was also preferred to models that use empirical relation between diffusivity and period of cure and relative humidity [49, 50] because of relative humidity dependence on hydration degree. Other research works showed that the drying-hydration phenomena can be modeled as a two stage process in which the material skin can be damaged [51].

4.1 Model description

In the model proposed, drying and hydration are treated in two different parts. The evolution of hydration has been determined using the programming language *Python*. This choice has been motivated by the fact that *Python* ensures the link between hydration and transport programs. Drying is calculated with *PyTOUGH* [52] that is a *Python* application programming interface for *TOUGH2* [53], a simulator for nonisothermal multiphase flow in fractured porous media. The numerical treatment of the simultaneous processes of phase flow and transport and hydration was handled using a sequential non-iterative split operator. Hence, for each time step defined by user the drying process was simulated. Then, the hydration program before a new drying process calculation actualized the liquid saturation and the transport properties.

4.1.1 Multiphase flow part

The physics of drying has been studied for a long time for porous materials. A classical approach is to consider that the transport of water (in liquid and gaseous phases) can be expressed as a pure fickian process [54]. It assumes that the gas pressure of the vapor-air mixture remains constantly equal to the outer atmospheric pressure. Nevertheless, although recent studies show that this approach is acceptable for concrete with small porosity and for external relative humidity greater than 20–30 % that is to say for most of cementitious materials in European latitudes [55], such a description cannot distinguish the role of both gaseous and liquid phases in the transport of water. This description is also a particular case of a more general one where moisture and air transport can be expressed as darcean and fickian transports in liquid and gas phases [56, 57].

Therefore, the equations of isothermal drying are derived from several laws, namely: the mass balance equations written for the liquid water phase, water vapor and dry air, the Fick's law governing the relative diffusion process of water vapor and dry air to the gaseous mixture, and the Darcy's law describing the transport of wet air and liquid water (see [tough2] for the complete equation system description).

This description assumes several hypotheses, namely:

- The gaseous phase is the result of the mix between two ideal gases (dry air and water vapor). The mix is also considered as ideal, thus the total gas pressure is equal to the sum of partial pressures of the two gases described before;
- The liquid phase is an incompressible pure water phase leading to the fact that diffusion is only present in the gaseous phase;
- Gravity forces are negligible compared to forces due to pressure;
- Although several studies show an heterogeneous temperature distribution at the structural scale [58], simulations are done at constant temperature considering that the sizes of the samples are sufficiently small to adopt such an hypothesis;
- Skeleton is incompressible and non-expansive (constant temperature).

It is important to note that the system of equations is described by the liquid pressure in the porous media that is independent of the concentration of ions in the solution unlike relative humidity.

The relative permeabilities of liquid and gas have been chosen to be expressed as a function of saturation (S_l), as proposed by Van Genuchten (see Eqs. (13), (14)):

$$k_{r_l} = \begin{cases} \sqrt{\tilde{S}}\left[1-\left(1-\tilde{S}^{1/\lambda}\right)^{\lambda}\right]^2 & \text{if } S_l < S_{l_s} \\ 1 & \text{if } S_l \geq S_{l_s} \end{cases} \quad (13)$$

With

$$\tilde{S} = (S_l - S_{lr})/(S_{ls} - S_{lr}) \quad (14)$$

S_{lr}, S_{ls}: The residual liquid saturation, and the liquid saturation at saturation.

The capillary pressure has also been expressed as a function of saturation (15):

$$P_c = -P_0\left(\left[\tilde{S}\right]^{-1/\lambda}\right)^{1-\lambda} \quad (15)$$

P_0, λ: Van Genuchten's parameters.

The substitution of the capillary pressure in the Kelvin-Laplace equation (see Eq. (9)) leads to the desorption isotherm relation. The desorption and adsorption isotherms were assumed to be the same.

Finally, the diffusion coefficients for water and air in the gas phase were expressed as follows:

$$D_g^i = \Phi\tau_0\tau_\beta\rho_\beta D_{g0}^i \quad (16)$$

$\tau_0\tau_\beta$: The tortuosity, which includes a porous medium dependent factor and a coefficient that depends on phase saturation

ρ_β: The density

D_{g0}^i: the diffusion coefficient of the mass component in free gas (without porous media).

The saturation dependence of tortuosity is not well known at present. Several model have been frequently used as the Millington and Quirk model [59]:

$$\tau_0\tau_\beta = \Phi^{1/3}S_\beta^{10/3} \quad (17)$$

Nevertheless, this expression yields non-zero tortuosity coefficients as long as phase saturation is non-zero. In addition, the exponents' values are not adapted for cementitious materials [55]. Finally, it stands to reason that diffusive flux should vanish when a phase becomes discontinuous at low saturations, suggesting that saturation-dependent tortuosity should be related to relative permeability, e.g., $\tau_\beta = k_{r\beta}$

The gas relative permeability:

$$K_{rg} = (1 - S^*)^2\left(1 - S^{*2}\right) \quad (18)$$

With $S^* = (S_l - S_{lr})/\left(1 - S_{lr} - S_{rg}\right)$

S_{rg}: The residual gas saturation.

This system, supplemented by initial and boundary conditions, is used thereafter in order to compare numerical results to experimental data for water transport in cementitious materials.

4.1.2 Hydration part [47]

Hydration appears in the sinks term of the mass balance equations written for the liquid water phase. The system of equations is described in details in Appendix 1. It is important to note that the material properties are different from one element to another, consequently the history and the evolution of those properties too.

4.2 Required input data

A 1-D radially symmetric geometry is used to model the samples. A simple mesh composed of one 60-element row was used and represented the radius of the samples. The time step was 24 h because simulations were not sensible to the time step.

Several input data are required to solve the system of equations, such as the transport properties (intrinsic permeability after curing stage k_{l_0}, relative permeability, initial porosity after mixing ϕ_0, and characteristic time of the diffusion regime), the properties relative to the hydration part of the model (initial hydration degree, critical moisture content under which hydration stops). In this study, hydration was supposed to stop at a critical relative humidity value of 70 % in the material [60, 61]. As the equivalent critical moisture content depends on the critical relative humidity, the porosity (that depends on hydration degree), and the desorption isotherm (see Eq. (9)), the critical moisture content was actualized at each time step.

The intrinsic bulk permeability k_l can be assessed by numerical inverse analysis. The method used here consists in comparing the relative mass loss versus time plots predicted by the proposed model and experimentally recorded [55]. Initial liquid saturation was also chosen in order to obtain the same ultimate mass loss as experimental results. The sample with the medium notional size of cross-section that was the more stable in terms of experimental mass loss evolution as a function of time was chosen to fit the experimental data (Initial relative humidity at 1 day 0.9 and initial intrinsic permeability $8E10^{-21}$ m^2 were deduced by inverse modeling).The value of mean radius of cement grains was 18×10^{-6}, and hydration degree after curing stage (24 h) was 0.4. The hydration degree of the studied concretes was not monitored. Previous studies on Portland cement based materials showed that the degree of hydration ranges from 0.35 to 0.50 [7, 62–64] at 24 h at 20 °C, i.e. at the end of curing in this study. Thus 0.4 is a relatively low value but SCC mixtures included water-reducing admixture, which is known to delay hydration at early ages.

4.3 Numerical results

4.3.1 Without taking into account the drying depth

A first simulation has been realized on SCC-N concrete with the proposed model. Initial parameters are given in Table 5. Figure 15a–d shows the results obtained by taking into account the hydration-drying coupling model for liquid saturation, hydration degree, intrinsic permeability and porosity as a function of depth at final time (800 days), respectively. Boundary conditions were imposed at $x = 0$. Negatives values represent concrete. Figure 15e, f expose the mass loss and the mass loss over notional size of cross-section ratio as a function of time, respectively. The four sets of curves show that the liquid saturation, hydration degree, porosity and permeability are dependent of the specimen sizes (see Fig. 15a–d). They also indicate that the model is able to simulate the hydration degree, porosity and permeability gradients and that the hydration can stop because of drying (see Fig. 15b–d). This latter result is confirmed by Fig. 16 that shows the hydration degree of the medium scale sample as a function of depth and time. The hydration degree of the outer layer remained close to the initial hydration degree until the end of the test.

Table 5 Calculated skin porosity for different concrete

Porosity	Ø78 mm (%)	Ø113 mm (%)	Ø163 mm (%)	Average (%)	Standard deviation (%)
SCC-N	17.8	17.4	16.6	17.3	0.4
SCC-R	16.6	16.2	16.0	16.3	0.2
SCC-G	18.0	17.1	17.0	17.4	0.4
VC	15.5	15.7	15.7	15.7	0.1

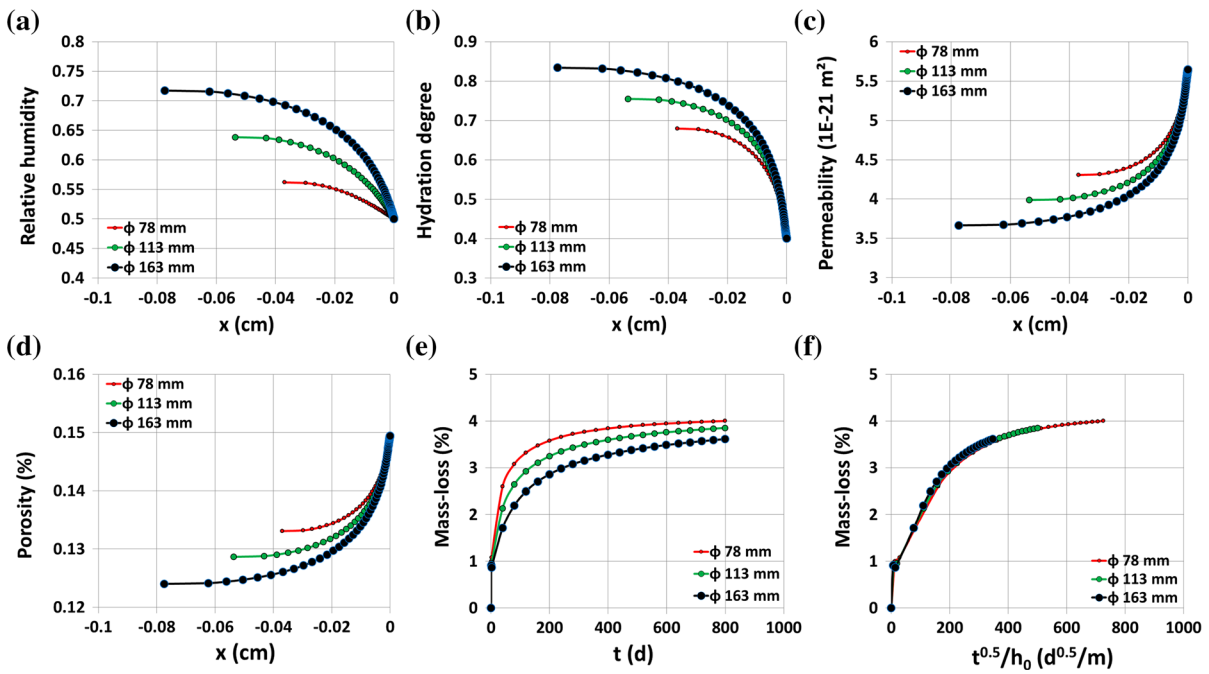

Fig. 15 Results of drying-hydration coupling for SCC-N for 3 different sample scales. **a** Relative humidity versus depth after 800 days of drying-hydration, **b** hydration degree versus depth after 800 days of drying-hydration, **c** permeability versus depth after 800 days of drying-hydration, **d** porosity versus depth after 800 days of drying-hydration, **e** mass loss evolution versus time, **f** mass loss evolution versus $\frac{\sqrt{t}}{h_0}$

Nevertheless, the simulation shows that the size effects on the mass loss observed experimentally could not be reproduced (see Fig. 15f). The different behaviors on porosity, permeability, liquid saturation, hydration degree were not sufficient to result in size effects.

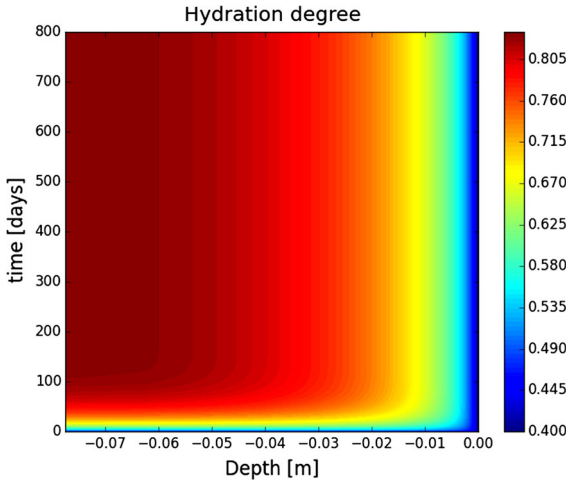

Fig. 16 Hydration degree as a function of depth and time for the medium scale SCC-N concrete

4.3.2 By taking into account the drying depth

In order to be able to reproduce numerically the size effects two other phenomena can be added to the model, namely: the so-called "skin" effect because the composition of concrete skin is different from the internal concrete, due to phenomena such as a contact with form works and segregation of aggregates [42, 43], and cracking during drying/hydration process [65]. For the first phenomenon a classical approach is to assume that the porosity and permeability are greater in the first millimeters of the samples because the superficial layer of concrete is mostly made of cement paste, which often tends to be more porous than bulk concrete [42]. Concerning the effect of cracking, the same assumption has been previously done in a simple two stage model for simulating drying shrinkage versus mass-loss evolution of concrete [51] and justified by experimental observations [66].

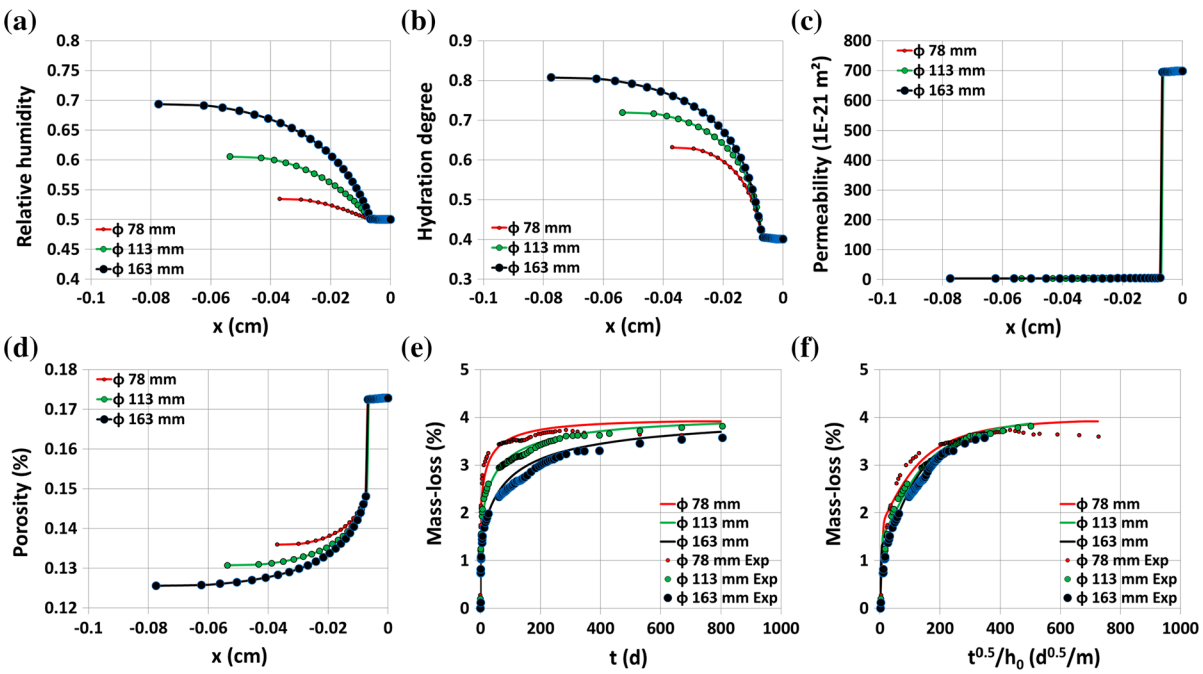

Fig. 17 Results of drying-hydration coupling for SCC-N for 3 different sample scales and with skin effect. **a** Relative humidity versus depth after 800 days of drying-hydration, **b** hydration degree versus depth after 800 days of drying-hydration, **c** permeability versus depth after 800 days of drying-hydration, **d** porosity versus depth after 800 days of drying-hydration, **e** mass loss evolution versus time, **f** mass loss evolution versus $\frac{\sqrt{t}}{h_0}$

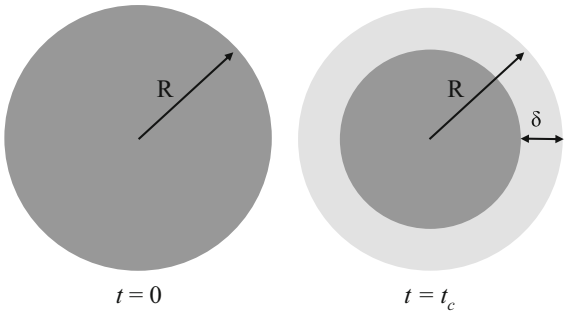

Fig. 18 Representation of the drying depth from $t = 0$ to $t = t_c$

Initial porosities ϕ_i were deduced from experimental determination of δ (see Table 4) by assuming the hydration does not significantly evolve in this layer where the porosity remains constant (see Appendix 3).

Then a simulation was performed assuming that the depth for which transport properties were different was the drying depth (see Sect. 3.3). For instance, this value was equal to 7.1 mm for the SCC-N concrete. Permeability arbitrary chosen to be 125 times greater in these first millimeters, which is a value that takes into account all "skin" effect. This value is very difficult to estimate and to the knowledge of the authors there is no data to confirm this hypothesis.

Figure 17f points out that such an assumption leads to the observation of size effects on the mass loss and confirms the tendency of experimental results. It also showed that the results agree well with the experimental results (d and f).

5 Conclusions

This paper analyzes the drying shrinkage and mass loss of concrete at long-term in order to study the size effects on kinetics and ultimate values. The shrinkage tests and mass loss measurements were performed on three self-consolidating concrete and one vibrated concrete. A numerical model coupling the hydration and drying of cementitious materials was used to understand the size effect observed on long-term drying. The analysis of the experimental and numerical results obtained leads to the following conclusions:

- The direct comparison of shrinkage magnitudes of different concrete mixtures at fixed drying time can be misleading, as shown by experimental results. Based on Torben's hyperbolic equation, the proposed approach provides two parameters from drying shrinkage tests: the ultimate value and the time to reach half of the ultimate value. Interpretation of the results becomes easier and more reliable.
- The ultimate drying shrinkage was not influenced by size effect, but the kinetics varied as a function of specimen size. This variation cannot be solely explained by the notional size of cross-section effect. The same observations were made on mass-loss curves.
- The existing shrinkage code models are based on a transport description with a solution expressed as a function of equivalent time t^* given by the square root of time to notional size of cross-section ratio. They usually perfectly describe the drying phenomena, but they do not take into account the complex phenomena-taking place when concrete is exposed to drying at early age. The heterogeneity of concrete and the evolution of its properties imply the existence of other phenomena, like hydration, wall effect, and micro cracking, which are not taken into account by classical models. The graphs plotted as a function of t^* confirm the existence of size effect involving these secondary phenomena not taken into account by the classical model.
- The analysis of drying shrinkage versus relative mass-loss curves showed three stages. The first stage corresponds to water loss without shrinkage. The relative mass loss triggering shrinkage was found dependent on the specimen size. This size effect was explained by the existence of a constant drying depth, where concrete can dry without generating shrinkage. The depth actually depended mainly on concrete mixture and was relatively not affected by specimen size. Several phenomena are likely to generate the drying depth: hydration-drying coupling, wall effect, and micro cracking. In order to conclude on the relative influence of these phenomena on overall size effect, a numerical study was performed.
- The drying model with a hydration part cannot reproduce the size effect observed experimentally. The integration of the "drying depth" notion in this modeling, with a higher porosity and a higher permeability than the internal concrete, gives better numerical results, with a good description of the size effect on the mass-loss curves.

A new approach was proposed in this article, which allows deducing the initial concrete boundary macroporosity from the shrinkage-mass loss curves. A drying depth was defined and the calculations of macroporosity values for different concrete mixtures were given. These new notions help understand the experimental differences observed between the specimen sizes. As the drying depth was found independent of the specimen size, this concept could be useful to take into account the effects of curing and early-age drying on durability of concrete structures.

Appendix 1: Hydration part

Hydration appears in the sinks term of the mass balance equations written for the liquid water phase and can be expressed as a quantity that is dependent of hydration degree for the water component [47]:

$$q = \frac{\mathrm{d}\alpha}{\mathrm{d}t}\lambda C \tag{19}$$

where C is the initial cement content [kg/m^3] and the consumed water mass per mass of hydrated cement [47]. The time derivative of the hydration degree can be written as follows:

$$\frac{d\alpha}{dt} = \frac{3D}{R^2}\frac{(1-\alpha)^{2/3}}{(1-\alpha^D)^{1/3}-(1-\alpha)^{1/3}} H\left(\phi_l - \phi_l^{cr}\right)\frac{\phi_l - \phi_l^{cr}}{\phi_l^0 - \phi_l^{cr}} \tag{20}$$

where $D, R, \alpha^D, \phi_l, \phi_l^0, \phi_l^{cr}$ denote the diffusion coefficient of ionic species through the hydrated coating around the clinker grains, the mean radius of the initial cement grains, critical hydration degree, moisture content, initial moisture content and critical moisture content that corresponds to the lower limit under which hydration stop, respectively denotes the Heaviside function.

Porosity was actualized as follows (21):

$$\Phi = \Phi_0\left(1 - \alpha\frac{\mu C}{E}\right) \tag{21}$$

With μ, C and E the quantity of water consumed by weight of cement, the initial cement and water contents, respectively is the initial porosity (after mixing).

Finally, the actualization of the intrinsic permeability reads:

$$k_l = k_{l0}\left(\frac{\Phi}{\Phi_0}\right)^2\left(\frac{1-\Phi_0}{1-\Phi}\right)^2 \tag{22}$$

The relative permeabilities are assumed to be independent of the hydration degree [47].

Appendix 2: numerical procedure

In the model proposed, drying and hydration are treated in two different parts. The evolution of hydration has been determined using the programming language *Python* based on the work of Nguyen et al. [40, 47]. This choice has been motivated by the fact that *Python* ensures the link between hydration and transport programs. Drying is calculated with *PyTOUGH* [52] that is a *Python* application programming interface for *TOUGH2* [53], a simulator for nonisothermal multiphase flow in fractured porous media. The numerical treatment of the simultaneous processes of phase flow and transport and hydration was handled using a sequential non-iterative split operator. Hence, for each time step defined by user the drying process was simulated. Then, the hydration program before a new drying process calculation actualized the liquid saturation and the transport properties.

For the resolution, hydration degree is calculated at time step n whereas mass and fluxes are calculated at time $n+1$ (see Eq. (23)). Hence, no iteration scheme is used, leading to faster simulations.

$$\left(\frac{d}{dt}M_i\right)^{n+1} = \left(\Delta F^i\right)^{n+1} + \left(q^i\right)^n \tag{23}$$

Equation (20) is nonlinear because of the presence of the hydration degree in the right part of the equation and because the moisture content depends on the hydration degree. This ordinary differential equation was then solved by an iterative procedure until convergence.

A 1-D radially symmetric geometry is used to model the samples. A simple mesh composed of one 60-element row was used and represented the radius of the samples. The time step was 24 h because simulations were not sensible to the time step.

Appendix 3: computation of the skin's initial porosity

Initial porosities ϕ_i were deduced from experimental determination of δ (see Table 4) by assuming the

hydration does not significantly evolve in this layer where the porosity remains constant. The drying depth δ corresponds to the initial mass loss Δm_0 for which shrinkage starts. If V_{eva} is the evaporated water and V_{dry} is the drying volume of concrete corresponding to the drying depth δ we can write (24):

$$\phi_i \cdot v_{dry} = v_{eva} \tag{24}$$

Developing Eq. (24) for a cylindrical specimen reads:

$$\left(\pi R^2 - \pi(R-\delta)\right)^2 h = \frac{\Delta m_0}{\phi_i \rho_e} \tag{25}$$

ρ_e: Water density (kg/m^3)h The height of the specimen's mass-loss measurement (m)

The initial porosity reads:

$$\Phi_i = \frac{\Delta m_0}{\rho_e\left(\pi R^2 - \pi(R-\delta)^2\right)h} \tag{26}$$

The gathers the values of initial porosity. The calculated porosity was based on the estimation of the drying capillary pores. Saturated micropores were not taken into account in Eq. (26). At 50 % of relative humidity, the corresponding pores radius given by Kelvin Laplace equation considering the adsorbed water is 2 nm [67]. Below this value, the pores were saturated. This fraction of concrete porosity was assumed to have no significant influence on the long-term drying behavior under our experimental conditions.

The porosity of the drying depth depends clearly on the concrete mixture. For instance the porosity of *SCC-N* was higher than the porosity of other concretes, and it concerned a deeper layer. The *SCC-N* concrete actually had higher proportion of limestone filler addition and lower cement content thus high free water content. The VC concrete showed lower initial porosity in spite of relatively high water-to-cement ratio, because of lower volume of paste.

References

1. Rozière E, Granger S, Turcry P, Loukili A (2007) Influence of paste volume on shrinkage cracking and fracture properties of self-compacting concrete. Cem Concr Compos 29(8):626–636
2. Saliba J, Rozière E, Grondin F, Loukili A (2011) Influence of shrinkage-reducing admixtures on plastic and long-term shrinkage. Cem Concr Compos 33(2):209–217
3. Darquennes A, Rozière E, Khokhar MIA, Turcry P, Loukili A, Grondin F (2012) Long-term deformations and cracking risk of concrete with high content of mineral additions. Mater Struct 45(11):1705–1716
4. Bazant ZP, Hubler MH, Wendner R, Yu Q (2013) Progress in creep and shrinkage prediction engendered by alarming bridge observations and expansion of laboratory database. In: Proceedings of the ninth international conference on creep, shrinkage, and durability mechanics (Concreep-9)
5. Bentur A, Mitchell D (2008) Material performance lessons. Cem Concr Res 38(2):259–272
6. Samouh H, Rozière E, Loukili A (2015) Influence of formwork duration on shrinkage, microstructure, and durability of cement based materials, in ConCreep 2015
7. Samouh H (2015) Nouvelles approches des relations entre formulation et comportement différé des matériaux cimentaires: application aux bétons autoplaçants., Ecole Centrale de Nantes
8. Picandet V, Khelidj A, Bellegou H (2009) Crack effects on gas and water permeability of concretes. Cem Concr Res 39(6):537–547
9. Djerbi Tegguer A, Bonnet S, Khelidj A, Baroghel-bouny V (2013) Effect of uniaxial compressive loading on gas permeability and chloride diffusion coefficient of concrete and their relationship. Cem Concr Res 52:131–139
10. European standard (2004) *E*urocode 2: design of concrete structures EN1992-1-1, pp 1–250
11. Hooton RD, Bickley JA (2014) Design for durability: the key to improving concrete sustainability. Constr Build Mater 67:422
12. Keeton JR (1965) Study of creep in concrete, Technical reports R333-I, R333-II, R333-III. U.S. Naval civil engineering laboratory, Port Hueneme
13. Wallo CE, Yuan EM, Lott RL, Kesler JL (1965) Sixth progress report on prediction of creep in structural concrete from short time tests'. T & AM Report No. 658, Department of Theoretical and Applied Mechanics, University of Illinois at Urbana
14. Torben C, Hansen W, Mattock AH (1966) Influence of size and shape of member on the shrinkage and creep of concrete. J Am Concr Inst 63(10):267–290
15. Almudaiheem J, Hansen W (1987) Effect of specimen size and shape on drying shrinkage of concrete. ACI Mater J 84:130–135
16. Almudaiheem J, Hansen W (1989) Prediction of concrete drying shrinkage from short-term measurements. ACI Mater J 86:401–408
17. Hansen W, Almudaiheem J (1987) Ultimate drying shrinkage of concrete-influence of major parameters. ACI Mater J 84:217–223
18. Bazant ZP, Wittmann FH, Kim JK, Alou F (1987) Statistical extrapolation of shrinkage data-part I: regression. ACI Mater J 84:20–34
19. Bazant Z, Kim JK, Wittmann FH, Alou F (1987) Statistical extrapolation of shrinkage data—part II: bayesian updating. ACI Mater J 84:83–91
20. Miyazawa S, Tazawa E (2001) Influence of specimen size and relative humidity on shrinkage of high-strength concrete. Concr Sci Eng 3(March):39–46
21. Van Breugel K, Ouwerkerk H, Industry RC, De Vries J (2000) Effect of mixture composition and size effect on shrinkage of high strength concrete. RILEM 2000:161–177

22. fib (2013) fib Model Code for Concrete Structures 2010. Ernst & Sohn, E34 pp
23. RILEM TC 107-GCS (1995) Creep and shrinkage prediction model for analysis and design of concrete structures - model B3. Mater Struct 28:357–365
24. ACI Committee 209 (2008) Guide for modeling and calculating shrinkage and creep in hardened concrete. Report No. 209.2R-08, pp 45
25. Wendner R, Hubler MH, and Bazant ZP (2013) The B4 model for multi-decade creep and shrinkage prediction. In: Proceedings of the ninth international conference on creep, shrinkage, and durability mechanics (Concreep-9), pp 429–436
26. Torrenti JM, Benboudjema F (2013) Dessiccation shrinkage of large structures: is there a size effect?. In: Proceedings of the ninth international conference on creep, shrinkage, and durability mechanics (Concreep-9), no. 1966, pp 404–411
27. Benboudjema F, Meftah F, Torrenti JM (2005) Interaction between drying, shrinkage, creep and cracking phenomena in concrete. Eng Struct 27(2):239–250
28. Spinner E, Teft W (1961) A method for determining mechanical resonance frequencies and for calculating elastic modulus from these frequencies. In: Proceedings of the ASTM, 1961
29. R. T. 107-CSP (1998) Measurement of time-dependent strains of concrete. Mater Struct 31:507–512
30. Grasley ZC, Lange DA, D'ambrosia MD, Villalobos-chapa S (2006) Relative humidity in concrete. ACI Comm 236:51–57
31. Baroghel-bouny V, Godin J (2001) Experimental study on drying shrinkage of ordinary and high-performance cementitious materials. RILEM Conf Shrinkage 3(9):13–22
32. Mokarem DW, Weyers RE, Lane DS (2005) Development of a shrinkage performance specifications and prediction model analysis for supplemental cementitious material concrete mixtures. Cem Concr Res 35(5):918–925
33. ACI Committee 209 (1997) Prediction of creep, shrinkage, and temperature effects in concrete structures. Report No. 209R-92, pp 47
34. Kristiawan SA, Sangadji S (2009) Prediction model for shrinkage of lightweight aggregate concrete. ASIAN J Civ Eng 10(5):549
35. L'Hermite RG, Mamillan M (1970) Influence de la dimension des éprouvettes sur le retrait. Ann Inst Techn Bâtiment Trav Publics 23:5
36. F Benboudjema, J Torrenti (2011) Prediction of drying shrinkage in concrete structures: study of size effect. In: International RILEM conference on advances in construction materials through science and engineering, pp 288–293
37. Bissonnette B, Pierre P, Pigeon M (1999) Influence of key parameters on drying shrinkage of cementitious materials. Cem Concr Res 29(July):1655–1662
38. Torrenti M, Granger L, Diruy M, Genin P (1999) Modeling concrete shrinkage under variable ambient conditions. ACI Mater J 96:35–39
39. Therrien J, Bissonnette B, Cloutier A (2000) Early-age evolution of the mass transfer properties in mortar and its influence upon ultimate shrinkage. In: International RILEM workshop on shrinkage of concrete (Shrinkage 2000), pp 247–268
40. Nguyen MD, Thiery M, Belin P (2013) A model for hydration-drying interactions in the concrete cover. In: Thermo-hydromechanical and chemical coupling in geomaterials and applications: proceedings of the 3 international symposium GeoProc'2008
41. de Sa C, Benboudjema F, Thiery M, Sicard J (2008) Analysis of microcracking induced by differential drying shrinkage. Cem. Concr Compos 30(10):947–956
42. Kreijger PC (1972) The skin of concrete Composition and properties. Mater Constr 17:275–283
43. Andrade C, Dı JM, Alonso C (1997) Mathematical modeling of a concrete surface 'skin effect' on Diffusion in chloride contaminated media. Adv Cem Based Mater 6:39–44
44. Al-Saleh SA, Al-Zaid RZ (2006) Effects of drying conditions, admixtures and specimen size on shrinkage strains. Cem Concr Res 36(10):1985–1991
45. Idiart AE, López CM, Carol I (2010) Modeling of drying shrinkage of concrete specimens at the meso-level. Mater Struct 44(2):415–435
46. Gawin D, Pesavento F, Schrefler BA (2006) Hygro-thermo-chemo-mechanical modelling of concrete at early ages and beyond. Part I: hydration and hygro-thermal phenomena. Int J Numer Methods Eng 67(3):299–331
47. Nguyen MD (2009) Modélisation des couplages entre hydratation et dessiccation des matériaux cimentaires à l'issue du décoffrage, PhD Ecole Nationale des Ponts et Chaussées, France
48. Bentz DP, Hansen KK, Madsen HD, Vallée F, Griesel EJ (2001) Drying/hydration in cement pastes during curing. Mater Struct 34(November):557–565
49. Haouas A (2007) Comportement au jeune âge des matériaux cimentaires-Caractérisation et modélisation chimio-hydro-mécanique du retrait, PhD Ecole Normale Supérieure de Cachan, France
50. Buffo-Lacarrière L, Sellier A, Escadeillas G, Turatsinze A (2007) Multiphasic finite element modeling of concrete hydration. Cem Concr Res 37(2):131–138
51. Delaplace A, Noyalet H (2013) A simple two-stage model for simulating drying shrinkage vs. Mass-loss evolution of concrete. In: VIII international conference on fracture mechanics of concrete and concrete structures FraMCoS-8
52. Croucher A (2011) Pytough: a python scripting library for automating tough2 simulations. In: New Zealand geothermal workshop 2011 proceedings,No. Nov
53. Pruess K, Oldenburg C, Moridis G (1999) Tough2 user's guide, version 2, no. November 1999
54. Bazant ZP, Najjar LJ (1972) Nonlinear water diffusion In nonsaturated concrete. Mater Constr 5:3–20
55. Thiery M, Baroghel-bouny V, Bourneton N, Villain G, Stéfani C (2007) Modélisation du séchage des bétons-Analyse des différents modes de transfert hydrique. Rev Eur GENIE Civ 11:541–577
56. Mainguy M, Coussy O, Baroghel-bouny V (2001) Role of air pressure in drying of weakly permeable materials. J Eng Mech 127:582–592
57. Coussy O (2003) Poromechanics. Wiley, pp 312
58. Park K, Jee N, Yoon I, Lee H (2008) Prediction of temperature distribution in high-strength concrete using hydration model. ACI Mater J 105:180–186

59. Millington R, Quirk JP (1961) Permeability of porous solids. Trans Faraday Soc 57(8):1200–1207
60. City Q, Adam T, Kroggel O, and Gruebl P (2006) Influence of the relative humidity on the hydration kinetics of concrete. In: 2nd international symposium on advances in concrete through science and engineering 11–13 Sept 2006, Quebec City, no. Sept
61. Loukili A, Khelidj A, Richard P (1999) Hydration kinetics, change of relative humidity, and autogenous shrinkage of ultra-high-strength concrete. Cem Concr Res 29(4):577–584
62. Cortas R, Rozière E, Staquet S, Hamami A, Loukili A, Delplancke-Ogletree M-P (2014) Effect of the water saturation of aggregates on the shrinkage induced cracking risk of concrete at early age. Cem Concr Compos 50:1–9
63. Bentz DP (1997) Three-dimensional computer simulation of portland cement hydration and microstructure development. J Am Ceram Soc 80(1):3–21
64. Escalante-Garcia J (2003) Nonevaporable water from neat OPC and replacement materials in composite cements hydrated at different temperatures. Cem Concr Res 33(11):1883–1888
65. Bazant ZP, Raftshol WJ (1981) Effect of cracking in drying and shrinkage specimens. Cem Concr Res 12:209–226
66. Bakhshi M, Mobasher B (2011) Experimental observations of early-age drying of Portland cement paste under low-pressure conditions. Cem Concr Compos 33(4):474–484
67. Ranaivomanana H, Verdier J, Sellier A, Bourbon X (2011) Toward a better comprehension and modeling of hysteresis cycles in the water sorption–desorption process for cement based materials. Cem Concr Res 41(8):817–827